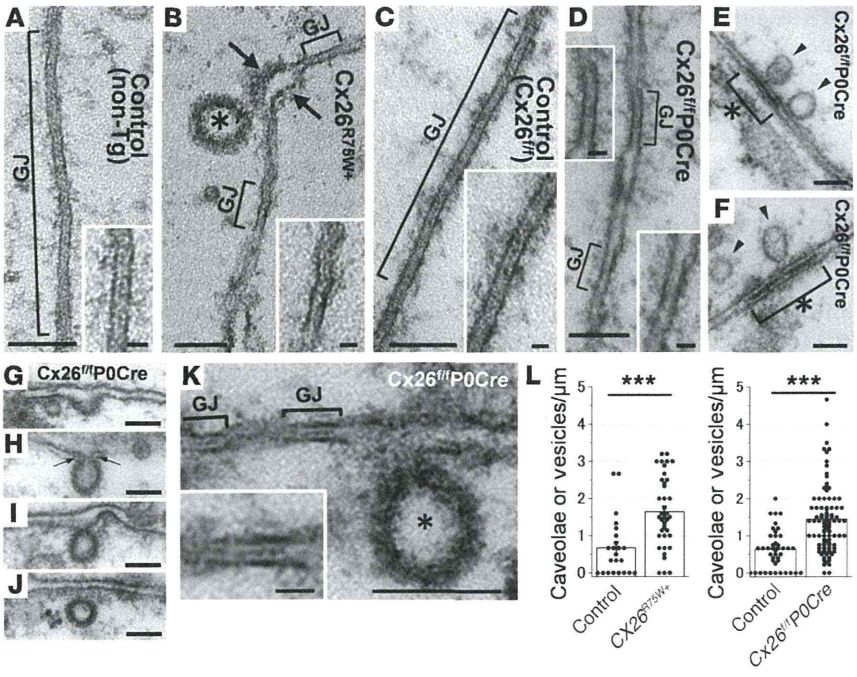

Figure 6
Discontinuous gap junctions with excessive endocytosis in CX26-mutant mice. (**A**–**K**) Ultrastructure of gap junctions and caveolae in 5-week-old *CX26^{R75W+}* (**B**) and *Cx26$^{f/f}$ P0-Cre* (**D**–**K**) mice compared with their respective littermate controls (**A** and **C**). Horizontal ultrathin sections of ISCs revealed that most of the gap junctions (GJs, brackets) were remarkably shorter or discontinuous (**B**, **D**, and **K**) compared with those of the control ISCs (**A** and **C**). (**B**) A caveolar vesicle (asterisk) with dissociated plasma membrane (arrows) around a short gap junction in a *CX26^{R75W+}* mouse. In both mutant mice, numerous caveolae and vesicles (**B** and **K**, asterisks; **E** and **F**, arrowheads; **G**–**J**) were observed. (**E** and **F**) Abnormally condensed intermembrane layers (asterisks with brackets) at the cell borders were observed in *Cx26$^{f/f}$ P0-Cre* mice. (**G**–**J**) In *Cx26$^{f/f}$ P0-Cre* mice, the plasma membrane showed a small cave-like shape (**G**), an invagination with a neck (**H**, arrows), and the formation of a vesicle-like structure (**I**); the vesicle was separated from the plasma membrane (**J**). (**K**) A caveolar vesicle (asterisk) is shown at the edge of discontinuous short gap junctions (inset) with clear internal layers. (**L**) Number of caveolae or caveolar vesicles that were counted around each cell border (mean ± SEM with dot plots): n = 23 and 39 cells for the littermate control and *CX26^{R75W+}* mice, respectively (***$P = 3.2 \times 10^{-5}$); n = 42 and 97 for the littermate control and *Cx26$^{f/f}$ P0-Cre* mice, respectively (***$P = 8.4 \times 10^{-10}$). Scale bars: 100 nm and 20 nm (insets).

With regard to this drastic GJP disruption, we hypothesized that the abnormal GJPs in both CX26-mutant mice populations were triggered by abnormalities in the formation of the protein complex associated with CX26 and that the resultant molecular changes could lead to the disruption of GJP formation. As for internalization of CX26 protein, we fractionated the cochlear proteins and analyzed them by immunoblotting. CX26 from CX26R75W$^+$ mice was, however, distributed in the plasma membrane fraction, as was CX26 from the control mice (Supplemental Figure 10A). To determine the affinity for other connexins or connexons, we performed coimmunoprecipitation using CX26 antibodies. CX30 was detected in both the CX26R75W$^+$ mice and control mice, and thus no substantive abnormality in the CX26-CX30 interaction in the macromolecular complex could be demonstrated (Supplemental Figure 10B). To examine the interactions with the cytoskeleton, we performed several in vitro experiments with cytochalasin D treatment, which destroys the cytoskeleton, in HEK cells transfected with CX26-EGFP with or without the R75W mutation. We did not, however, observe an effect on GJP formation resulting from disruption of the cytoskeleton (data not shown). As for ubiquitination and autophagy of the GJP, including CX26, we examined the association of ubiquitination and autophagy with GJP disruption in CX26 mutants by immunoblot analysis and transmission electron microscopy. We could not find convincing evidence to show that these processes were more prevalent in CX26-mutant cochleae than in control cochleae (data not shown). As for membrane retrieval at cell junctions, our ultrastructural pathology demonstrated that a significantly larger number of caveolae and vesicles were associated with the cell border (including small gap junctions) in *Cx26$^{f/f}$P0-Cre* mice as compared with those in the control mice (Figure 6). This may indicate that excessive endocytosis occurs in the presence of this CX26 mutation, leading to membrane retrieval that may accelerate GJP degradation.

Discussion

In this study, we demonstrated a novel molecular pathology in the cochlea, that of degradation of the gap junction macromolecular complex in CX26-associated deafness, as well as a novel mechanism of GJP formation into one of two types (L-GJPs or S-GJPs) that is dependent on CX26 expression. These findings were consistent not only in cochlear cells, but also in a human cell line with artificial connexin expression. Our data suggest that both the dominant-negative R75W mutation and the absence of CX26 affect the accumulation and assembly of gap junction units in the cell-cell junctions between cochlear supporting cells.

Regarding the initial phenotype of the hearing organ in the connexin mutants (Figure 1 and Supplemental Figure 4), we have previously described an early histological change in CX26-mutant mice, which showed an absence of the small space needed to form the future tunnel of Corti around P5 (15). As for hearing function, the earliest change detected by the auditory brainstem response occurs only after P11 (15), because hearing input to the mouse cochlea normally begins between P11 and P12 (25). With respect to the function of the cochlear gap junction, Ca^{2+} responses fail to propagate in organotypic cultures with defective expression of CX26 or CX30 from P3 through P6 (26). Thus, to the best of our knowledge, the phenotype at the embryonic stage shown in the present study (Figure 1 and Supplemental Figure 4) has not been previously reported.

The mosaicism generated by our newly developed *Cx26$^{f/f}$P0-Cre* mice revealed that the formation of L-GJPs versus S-GJPs critically depended on CX26 expression, and CX26 expression from both adjacent cells was essential to form normal L-GJPs — even if CX30 was highly expressed in the same cells (Figure 1, D and E). The in vivo (Figure 3) and in vitro (Figure 4) findings concerning GJP formation provided conclusive evidence demonstrating that the formation of

L-GJPs has a definite CX26 dependency and that CX26 is required to form the large macromolecular complex of gap junctions.

Regarding the association between connexins and caveolins (Figure 5 and Supplemental Figure 9), gap junction activity is regulated by protein kinase Cγ activity associated with CAV1-containing lipid rafts (27). Connexin family members (including CX26) are targeted to lipid raft domains, where they interact directly with caveolins such as CAV1 (28). Interestingly, in that experimental system, CX26 was targeted to lipid rafts only when CX26 was coexpressed with CAV1, suggesting that CAV1 recruits CX26 to lipid rafts, although other connexins such as CX32, CX36, CX43, and CX46 showed this lipid raft targeting without any artificial expression of CAV1 (28). These data showing that CX26 is excluded from the lipid raft fraction are in agreement with our present observation that the lipid raft signals in *Cx26$^{f/f}$ P0-Cre* mice localized between S-GJPs with no regularity and with more diffuse labeling and less clarity compared with those in control mice (Supplemental Figure 9). This suggests that the partial targeting to lipid rafts of connexins such as CX30 occurred to prevent the assembly or reassembly of GJPs in CX26-mutant mice.

In many tissues, CX26 is often coexpressed with another connexin in individual cells (29), and it can form heterotypic channels containing homomeric or heteromeric channels with CX30 (10). Hearing loss caused by CX30 deficiency in mice is rescued by the overexpression of CX26 (30). This observation demonstrates that CX26 can compensate for CX30. In contrast, when CX26 is absent in conditional CX26-null mice, CX30 overexpression does not rescue the severe hearing loss (31). Thus, it was concluded that CX26 plays an essential role in the development of the auditory sensory epithelium and that its unique developmental functions required for normal hearing cannot be replaced by CX30 (31). In lens fiber cells, although the expression of CX46 and CX50 overlap extensively, mice that lack one or the other of these connexins (and that serve as a model system for cataract formation) exhibit different phenotypes (32, 33). Macromolecular complex degradation in GJPs that affects other partner connexins and critically reduces functional plaque area may explain not only hearing loss, but also conditions such as cataracts resulting from gap junction dysfunctions with uncompensated connexin mutations.

Until now, hereditary deafness with connexin mutations was believed to be initiated by a single molecular dysfunction or dominant-negative effect on the connexin partners (34), and the primary pathology had never been observed at the embryonic stage. As for the cell degeneration in the connexin mutants, Liang et al. reported that cell degeneration was not a primary cause of CX26 deficiency–associated hearing loss (35). Using a CX26-deficient mouse model similar to the one used in the present study, they demonstrated that cochlear cells, including spiral ganglion neurons, had no significant degeneration throughout postnatal development, although auditory brainstem responses (ABRs) were absent in the whole frequency range (8–40 kHz) after birth.

Here, we demonstrate that connexin-associated deafness, which is the most frequent type of hereditary deafness, may be initiated not by a single molecular dysfunction of connexins, but by a macromolecular complex degradation of GJPs from the embryonic stage. This loss of GJP area may then abolish the proper ionic gradient needed for intercellular communication in the cochlea.

To the best of our knowledge, this is the first report demonstrating that a mutation in CX26 induces macromolecular degradation of large gap junction complexes accompanied by an increase in caveolar structures, which may lead to excessive membrane retrieval and result in a drastic reduction in the GJP area. This may represent a new molecular pathology for hereditary sensorineural deafness and for the general formation of gap junctions, and thus this machinery could be an effective target for drug design and chemical screening to reinforce the assembly of the other cochlear connexins such as CX30.

Methods

Dominant-negative CX26R75W (CX26^{R75W+}) transgenic mice. *CX26^{R75W+}* mice were obtained from a breeding colony of a previously reported line (16). *CX26^{R75W+}* mice were maintained on a C57BL/6J background and crossed with C57BL/6J animals to generate R75W transgenic offspring. Nontransgenic (non-Tg) littermates on a C57Bl/6J background were always used as the control for *CX26^{R75W+}* mice.

Generation of novel conditional knockout mouse for CX26. A targeting vector of a floxed *Cx26* allele including exons 1 and 2 was constructed using phage DNA clones from a genomic library of J1 ES cells. An approximately 8.4-kb HindIII-BamHI fragment with exon 1 and a 2.85-kb SacI-SacI fragment containing the 3′ half of exon 2 were isolated and used to construct a targeting vector with long and short homologous sequences, respectively. One loxP sequence was introduced at the end of intron 1, and a Neo cassette was introduced between two loxP sequences in exon 2. The diphtheria toxin A (DT-A) chain expression cassette was used as a negative selection marker. The linearized targeting vector was introduced into J1 ES cells by electroporation, and G418-resistant clones were analyzed by Southern blotting to isolate the homologous recombinant as described (18, 36). Identified recombinant ES cells were injected into C57/BL6J blastocysts. A mouse strain harboring the floxed *Cx26* allele was established by crossing chimeras with C57/BL6J females to produce F1 heterozygotes (*Cx26$^{flox/+}$*). F2 offspring were generated by crossing F1 heterozygotes, and their genotyping was performed by PCR amplification. No apparent abnormalities were detected in the *Cx26$^{f/f}$* mice. Otic vesicle–specific CX26-knockout mice were generated by breeding *Cx26$^{f/f}$* mice with mice that expressed the Cre recombinase gene under the control of the promoter of the *P0* gene (*P0-Cre* mice, on a C57BL/6J background), as described (18). To evaluate Cre recombinase expression and distribution, P0-Cre mice were crossed with ROSA26-GFP reporter mice (Gt-ROSA-26sortm1sor, R26R), and the four mice from two litters were analyzed by fluorescence and confocal microscopy (Supplemental Figure 2). *Cx26$^{f/f}$* on a C57Bl/6J background in the littermates was always used as the control for the *Cx26$^{f/f}$ P0-Cre* mice.

Immunohistochemistry. Mice were anesthetized, killed, and the inner ear tissues were removed. The cochleae were further dissected and fixed in 4% PFA. Immunofluorescence staining with antibodies against CX26 (rabbit IgG from Life Technologies and mouse IgG from LifeSpan Biosciences), CX30 (rabbit IgG; Life Technologies), caveolin 1 (mouse IgG; BD Biosciences), and caveolin 2 (mouse IgG; BD Biosciences) was performed on whole-mount preparations of the finely dissected organ of Corti or cochlear cryosections (5-μm) that included ISCs. We incubated the tissues in the antibody solutions for 1 hour after blocking. The following secondary antibodies were used: Cy3-conjugated anti-rabbit IgG (Sigma-Aldrich) for anti-CX26 or -CX30 rabbit antibodies; Alexa Fluor 488–conjugated anti-mouse IgG (Life Technologies) for anti-CX26 mouse antibodies; Alexa Fluor 594–conjugated anti-mouse IgG (Life Technologies) for anti-CAV1 or -CAV2 mouse antibodies; and Alexa Fluor 633–conjugated anti-rabbit IgG (Life Technologies) for CX30 in double or triple staining. Lipid rafts were visualized with Alexa Flour 594–conjugated cholera toxin subunit B (CTxB, Life Technologies). Fluorescence confocal images were obtained with an LSM510-META confocal microscope (Zeiss). Some of the green fluorescence in *CX26^{R75W+}* mice indicates the pseudocolor obtained from

the Alexa Fluor 633–conjugated secondary antibody signal (Life Technologies), because these mice have ubiquitous EGFP expression from their transgene. *z*-stacks of images were collected at 0.5-μm intervals, and the single image stacks were constructed with the LSM Image Browser (Zeiss); three-dimensional images and videos were constructed using IMARIS software (Bitplane). We analyzed at least five samples from five animals at each age used, and representative images are shown. The compared images were photographed and processed using identical parameters. Three-dimensional images were constructed with *z*-stacked confocal images by IMARIS (Bitplane). Quantitative analysis of the GJP length (mean ± SEM) was performed with the LSM Image Browser (Zeiss), and data were compared using a Student's *t* test (Microsoft Excel).

Western blot analysis. The mouse cochlear proteins were extracted with T-PER Tissue Protein Extraction Reagent (Thermo Scientific) from at least six cochleae that included the organ of Corti, lateral wall, and stria vascularis. The proteins were resolved by SDS-PAGE with 4% to 20% mini-PROTEAN TGX gels (Bio-Rad Laboratories) and then transferred onto a PVDF membrane (Amersham Hybond-P; GE Healthcare). After blocking, the membranes were processed through sequential incubations with anti–caveolin 1 (1:1,000; BD) and anti–caveolin 2 (1:500; Sigma-Aldrich), rabbit anti-CX26 (1:1,000; Life Technologies), mouse anti-CX26 (1:1,000; LifeSpan Biosciences), and monoclonal anti–β-actin (1:1,500; Sigma-Aldrich) with HRP-conjugated anti-rabbit or anti-mouse IgG (1:40,000; GE Healthcare) as the secondary antibody. Amersham ELC Prime Western Blotting Detection Reagent (GE Healthcare) was then used for visualization, and the signal was developed on x-ray film (Amersham Hyperfilm ECL; GE Healthcare). Each experiment was repeated at least three times. Densitometric analysis of the band intensities was performed with ImageJ software (NIH). The data were normalized to the corresponding β-actin levels, expressed relative to the amount present in each littermate control, and compared using a Student's *t* test (Microsoft Excel).

Transmission electron microscopy. Animals were deeply anesthetized and perfused intracardially with 0.01 M PBS, followed by 2% PFA and 2% glutaraldehyde in 0.1 M cacodylate buffer. The cochleae were opened and flushed with the fixative for 2 hours at room temperature. After washing, the specimens were postfixed for 1.5 hours in 2% osmium tetroxide in 0.1 M phosphate buffer and then dehydrated through a graded ethanol series and embedded in Epon. Horizontal sections of the surface of the cochlear membrane labyrinth were cut, stained with uranyl acetate and lead citrate, and examined by electron microscopy (H-7100; Hitachi). The numbers of caveolae and vesicles were counted and compared using a Student's *t* test (Microsoft Excel).

Expression constructs and cell lines expressing CX26, CX30, or CX26 mutants. Expression constructs and cell lines were generated as previously described (10, 22). Briefly, human *GJB6* was obtained by RT-PCR (Superscript II; Life Technologies) from human corpus callosum RNA (Clontech) and subcloned into the pIRESpuro3 vector, then human *GJB2* was subcloned into the pIRESneo3 vector, and the *GJB2* mutations were introduced into the ORF of human *GJB2* cDNA by PCR site-directed mutagenesis using the QuickChange kit (Stratagene). Communication-incompetent HeLa cells were used to generate the stable cell lines expressing WT CX30. To generate cells expressing both WT CX30 and WT CX26 or CX26 mutants, one cloned cell line that stably expressed CX30 was transfected with *GJB2* in pIRESneo3. After selection with both 1 μg/ml of puromycin (Sigma-Aldrich) and 1 mg/ml of G418 (Life Technologies) for about 3 weeks, the colonies were trypsinized, and these bulk-selected cells were expanded for the subsequent studies. Quantitative analysis of GJP length (mean ± SEM) was performed with ImageJ software.

Immunocytochemistry and GJP quantification. HeLa cells were grown on coverslips for 2 days to a confluence of approximately 70% to 90%, fixed in acetone, and incubated with a monoclonal antibody (33-5800, diluted 1:500; Zymed Laboratories) and a rabbit antiserum against the C terminus of CX30 (71-2200, diluted 1:1,000; Zymed Laboratories); these did not cross-react with each other, as previously shown (10). The cells were visualized with tetramethylrhodamine isothiocyanate–conjugated (TRITC-conjugated) donkey anti-rabbit (Abcam) and FITC-conjugated donkey anti-mouse secondary antibodies (Abcam). The cells were photographed under a Leica fluorescence microscope with a Hamamatsu C4742-95 digital camera connected to a G5 Mac computer using OpenLAB 2.2 software for deconvolution. The images were analyzed for GJP length using ImageJ software. All GJPs from 30 to 35 cells of each cell line were measured, and the mean GJP length was compared between cells expressing CX30 alone and those expressing both CX30 and CX26, or between cells expressing both CX30 and CX26R75Q and those expressing both CX30 and CX26R75W, using a Student's *t* test (Stata).

Dye transfer with Scrape-loading. Dye transfer was investigated using a scrape-loading assay as previously described (10). Briefly, parental HeLa cells, bulk-selected cells that expressed WT CX30 alone, or cells that coexpressed WT CX30 and CX26 or one of the CX26 mutants (R75Q or R75W) were grown to confluence on coverslips. Following the scrape-loading with 2% NB and diffusion, the cells were washed, fixed, and the NB was visualized by TRITC-conjugated avidin (Sigma-Aldrich). Cells were photographed under a Leica fluorescence microscope with a Hamamatsu C4742-95 digital camera connected to a G5 Mac computer, using OpenLAB 2.2 software. Dye transfer was quantified by measuring the distance from the scrape line to the point where the average fluorescence intensity dropped to 1.5 times the background intensity. Eleven to twelve images were acquired from each of three different plates of cells. The images were processed and analyzed with ImageJ software, and the mean distance was calculated using Microsoft Excel software and compared using a Student's *t* test (Stata).

Statistics. A one-tailed Student's *t* test, with a significance criterion of $P < 0.05$, was used to compare the GJP length, relative protein levels, number of cells positive for accumulated caveolins, ABR thresholds, propagation ranges of Ca^{2+} signaling, distance of dye transfer, and number of caveolae or vesicles.

Study approval. All experimental protocols were approved by the IACUC of Juntendo University School of Medicine and were conducted in accordance with the NIH guidelines for the care and use of laboratory animals.

Acknowledgments

This work was supported in part by a research grant from the Ministry of Education, Science and Culture (JSPS KAKENHI 25462563, to K. Kamiya); the Ministry of Health, Labor and Welfare of Japan (to K.Kamiya); the MEXT support program for the Strategic Research Foundation at Private Universities, 2011–2012 (to K. Ikeda); the Terumo Life Science Foundation (to K. Kamiya); and by NIH grant KO8DC005394 (to S.W. Yum). We thank M. Yoshida at the Laboratory of Ultrastructure Research for help with the transmission electron microscopy; Y. Fujitani for providing the reporter mouse line; H. Mochizuki for providing the AAV; Y. Yokoyama and B. Kuerban for experimental assistance; the staff of the Division of Proteomics and Biomolecular Sciences for help with our proteomic analysis; and Y. Uchiyama for helpful advice.

Received for publication November 1, 2012, and accepted in revised form January 2, 2014.

Address correspondence to: Kazusaku Kamiya, Department of Otorhinolaryngology, Juntendo University Faculty of Medicine, Hongo 2-1-1, Bunkyo-ku, Tokyo 113-8421, Japan. Phone: 81.3.5802.1229; Fax: 81.3.5840.7103; E-mail: kkamiya@juntendo.ac.jp.

1. Chan DK, Schrijver I, Chang KW. Connexin-26-associated deafness: phenotypic variability and progression of hearing loss. *Genet Med.* 2010; 12(3):174–181.
2. Mason JA, Herrmann KR. Universal infant hearing screening by automated auditory brainstem response measurement. *Pediatrics.* 1998;101(2):221–228.
3. Petersen MB, Willems PJ. Non-syndromic, autosomal-recessive deafness. *Clin Genet.* 2006;69(5):371–392.
4. Morton NE. Genetic epidemiology of hearing impairment. *Ann N Y Acad Sci.* 1991;630:16–31.
5. Birkenhäger R, Lüblinghoff N, Prera E, Schild C, Aschendorff A, Arndt S. Autosomal dominant prelingual hearing loss with palmoplantar keratoderma syndrome: Variability in clinical expression from mutations of R75W and R75Q in the GJB2 gene. *Am J Med Genet A.* 2010;152A(7):1798–1802.
6. Kelsell DP, et al. Connexin 26 mutations in hereditary non-syndromic sensorineural deafness. *Nature.* 1997;387(6628):80–83.
7. Kikuchi T, Kimura RS, Paul DL, Takasaka T, Adams JC. Gap junction systems in the mammalian cochlea. *Brain Res Brain Res Rev.* 2000;32(1):163–166.
8. Ahmad S, Chen S, Sun J, Lin X. Connexins 26 and 30 are co-assembled to form gap junctions in the cochlea of mice. *Biochem Biophys Res Commun.* 2003;307(2):362–368.
9. Sun J, et al. Cochlear gap junctions coassembled from Cx26 and 30 show faster intercellular $Ca2^+$ signaling than homomeric counterparts. *Am J Physiol Cell Physiol.* 2005;288(3):C613–C623.
10. Yum SW, et al. Human connexin26 and connexin30 form functional heteromeric and heterotypic channels. *Am J Physiol Cell Physiol.* 2007; 293(3):C1032–C1048.
11. Beltramello M, Piazza V, Bukauskas FF, Pozzan T, Mammano F. Impaired permeability to Ins(1,4,5) P3 in a mutant connexin underlies recessive hereditary deafness. *Nat Cell Biol.* 2005;7(1):63–69.
12. Bukauskas FF, et al. Clustering of connexin 43-enhanced green fluorescent protein gap junction channels and functional coupling in living cells. *Proc Natl Acad Sci U S A.* 2000;97(6):2556–2561.
13. Gaietta G, et al. Multicolor and electron microscopic imaging of connexin trafficking. *Science.* 2002;296(5567):503–507.
14. Sosinsky G. Mixing of connexins in gap junction membrane channels. *Proc Natl Acad Sci U S A.* 1995;92(20):9210–9214.
15. Inoshita A, et al. Postnatal development of the organ of Corti in dominant-negative Gjb2 transgenic mice. *Neuroscience.* 2008;156(4):1039–1047.
16. Kudo T, et al. Transgenic expression of a dominant-negative connexin26 causes degeneration of the organ of Corti and non-syndromic deafness. *Hum Mol Genet.* 2003;12(9):995–1004.
17. Minekawa A, et al. Cochlear outer hair cells in a dominant-negative connexin26 mutant mouse preserve non-linear capacitance in spite of impaired distortion product otoacoustic emission. *Neuroscience.* 2009;164(3):1312–1319.
18. Hasegawa S, et al. Apoptosis in neural crest cells by functional loss of APC tumor suppressor gene. *Proc Natl Acad Sci U S A.* 2002;99(1):297–302.
19. Schutz M, et al. The human deafness-associated connexin 30 T5M mutation causes mild hearing loss and reduces biochemical coupling among cochlear non-sensory cells in knock-in mice. *Hum Mol Genet.* 2010;19(24):4759–4773.
20. Tritsch NX, Yi E, Gale JE, Glowatzki E, Bergles DE. The origin of spontaneous activity in the developing auditory system. *Nature.* 2007;450(7166):50–55.
21. Lang H, et al. Contribution of bone marrow hematopoietic stem cells to adult mouse inner ear: mesenchymal cells and fibrocytes. *J Comp Neurol.* 2006;496(2):187–201.
22. Yum SW, Zhang J, Scherer SS. Dominant connexin26 mutants associated with human hearing loss have trans-dominant effects on connexin30. *Neurobiol Dis.* 2010;38(2):226–236.
23. Zhang J, Scherer SS, Yum SW. Dominant Cx26 mutants associated with hearing loss have dominant-negative effects on wild type Cx26. *Mol Cell Neurosci.* 2011;47(2):71–78.
24. Uyguner O, et al. The novel R75Q mutation in the GJB2 gene causes autosomal dominant hearing loss and palmoplantar keratoderma in a Turkish family. *Clin Genet.* 2002;62(4):306–309.
25. Kamiya K, Takahashi K, Kitamura K, Momoi T, Yoshikawa Y. Mitosis and apoptosis in postnatal auditory system of the C3H/He strain. *Brain Res.* 2001;901(1-2):296–302.
26. Anselmi F, et al. ATP release through connexin hemichannels and gap junction transfer of second messengers propagate Ca2+ signals across the inner ear. *Proc Natl Acad Sci U S A.* 2008;105(48):18770–18775.
27. Lin D, Zhou J, Zelenka PS, Takemoto DJ. Protein kinase Cgamma regulation of gap junction activity through caveolin-1-containing lipid rafts. *Invest Ophthalmol Vis Sci.* 2003;44(12):5259–5268.
28. Schubert AL, Schubert W, Spray DC, Lisanti MP. Connexin family members target to lipid raft domains and interact with caveolin-1. *Biochemistry.* 2002;41(18):5754–5764.
29. Zhang JT, Nicholson BJ. The topological structure of connexin 26 and its distribution compared to connexin 32 in hepatic gap junctions. *J Membr Biol.* 1994;139(1):15–29.
30. Ahmad S, et al. Restoration of connexin26 protein level in the cochlea completely rescues hearing in a mouse model of human connexin30-linked deafness. *Proc Natl Acad Sci U S A.* 2007;104(4):1337–1341.
31. Qu Y, et al. Early developmental expression of connexin26 in the cochlea contributes to its dominate functional role in the cochlear gap junctions. *Biochem Biophys Res Commun.* 2012;417(1):245–250.
32. White TW, Goodenough DA, Paul DL. Targeted ablation of connexin50 in mice results in microphthalmia and zonular pulverulent cataracts. *J Cell Biol.* 1998;143(3):815–825.
33. Gong X, et al. Disruption of alpha3 connexin gene leads to proteolysis and cataractogenesis in mice. *Cell.* 1997;91(6):833–843.
34. Zhang Y, Tang W, Ahmad S, Sipp JA, Chen P, Lin X. Gap junction-mediated intercellular biochemical coupling in cochlear supporting cells is required for normal cochlear functions. *Proc Natl Acad Sci U S A.* 2005;102(42):15201–15206.
35. Liang C, Zhu Y, Zong L, Lu GJ, Zhao HB. Cell degeneration is not a primary causer for Connexin26 (GJB2) deficiency associated hearing loss. *Neurosci Lett.* 2012;528(1):36–41.
36. Shibata H, et al. Rapid colorectal adenoma formation initiated by conditional targeting of the Apc gene. *Science.* 1997;278(5335):120–123.

BMC Genetics

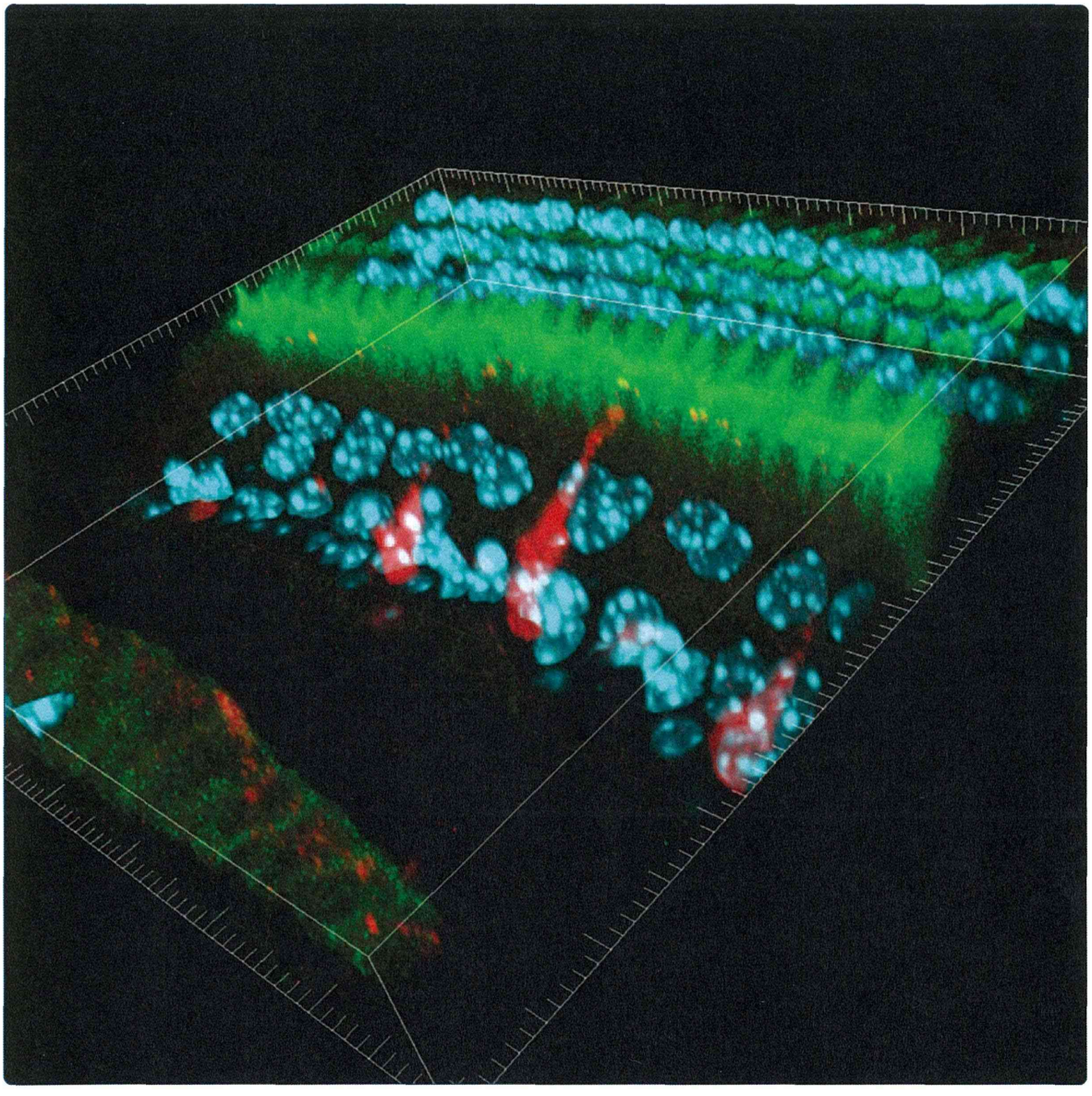

Dominant negative connexin26 mutation R75W causing severe hearing loss influences normal programmed cell death in postnatal organ of Corti

Inoshita *et al.*

BioMed Central

Inoshita *et al. BMC Genetics* 2014, **15**:1
http://www.biomedcentral.com/1471-2156/15/1

Inoshita et al. BMC Genetics 2014, 15:1
http://www.biomedcentral.com/1471-2156/15/1

BMC Genetics

RESEARCH ARTICLE Open Access

Dominant negative connexin26 mutation R75W causing severe hearing loss influences normal programmed cell death in postnatal organ of Corti

Ayako Inoshita, Keiko Karasawa, Megumi Funakubo, Asuka Miwa, Katsuhisa Ikeda and Kazusaku Kamiya*

Abstract

Background: The greater epithelial ridge (GER) is a developmental structure in the maturation of the organ of Corti. Situated near the inner hair cells of neonatal mice, the GER undergoes a wave of apoptosis after postnatal day 8 (P8). We evaluated the GER from P8 to P12 in transgenic mice that carry the R75W + mutation, a dominant-negative mutation of human *gap junction protein, beta 2, 26 kDa* (*GJB2*) (also known as *connexin 26* or *CX26*). Cx26 facilitate intercellular communication within the mammalian auditory organ.

Results: In both non-transgenic (non-Tg) and R75W + mice, some GER cells exhibited apoptotic characteristics at P8. In the GER of non-Tg mice, both the total number of cells and the number of apoptotic cells decreased from P8 to P12. In contrast, apoptotic cells were still clearly evident in the GER of R75W + mice at P12. In R75W + mice, therefore, apoptosis in the GER persisted until a later stage of cochlear development. In addition, the GER of R75W + mice exhibited morphological signs of retention, which may have resulted from diminished levels of apoptosis and/or promotion of cell proliferation during embryogenesis and early postnatal stages of development.

Conclusions: Here we demonstrate that Cx26 dysfunction is associated with delayed apoptosis of GER cells and GER retention. This is the first demonstration that Cx26 may regulate cell proliferation and apoptosis during development of the cochlea.

Keywords: Apoptosis, Hereditary hearing loss, Gjb2, Greater epithelial ridge, Mouse, Organ of corti

Background

Hereditary deafness affects about 1 in 2,000 children, and mutations in the *gap junction protein, beta 2, 26 kDa* gene (*GJB2*), also known as *connexin 26* (*CX26*), are the most common genetic causes of congenital bilateral non-syndromic sensorineural hearing loss. Gap junctions play important roles during the maturation and differentiation of developing tissues [1-5]. In the mammalian cochlea, we have demonstrated that a dominant-negative *GJB2* mutation results in incomplete postnatal development of the cochlear organ of Corti by R75W + transgenic mice, which carry a dominant-negative mutation of human *CX26* [6,7]. The organ of Corti in R75W + mice is reduced in height and has an increased midmodiolar-sectional area. In addition, several cochlear structures are absent in R75W + mice (including the tunnel of Corti, Nuel's space, and spaces surrounding the outer hair cells), and the number of microtubules within the inner pillar cells is significantly reduced. Morphometric changes in R75W + mice likely result from collapse of the organ of Corti and enlargement of support cells causing impaired distortion product otoacoustic emission [8], although the underlying mechanisms remain unclear.

The greater epithelial ridge (GER) is a developmental structure that is important during maturation of the organ of Corti in mice. Present at birth, the GER typically disappears by postnatal day 10 (P10) [9,10]. In the mouse, most apoptosis in the developing cochlear system occurs during embryogenesis [11]. In the developing

* Correspondence: kkamiya@juntendo.ac
Department of Otorhinolaryngology, Juntendo University Faculty of Medicine, Hongo 2-1-1, Bunkyo-ku, Tokyo 113-8431, Japan

spiral ganglion cells of rats, however, 22% of programmed cell death was measured between P5 and P6 [12]. We have shown that development of normal hearing function in C3H/HeJ mice requires a wave of programmed cell death in the GER from P7 to P12. We also observed mitosis in the GER after P7, indicating that GER cells are both degenerating and regenerating until their eventual elimination at P12 [13].

Here, we evaluated postnatal changes in the GER of *Gjb2* mutant mice. We report that a dominant-negative *Gjb2* mutation induced GER retention, indicating that *Gjb2*-dependant apoptosis is critical for formation of a functionally and morphologically normal auditory system.

Results

Programmed cell death with Caspase-3 activation in GER

To investigate whether the programmed cell death in GER of R75W + mice was affected, we performed whole mount immunostaining of the cochlea with anti-Cleaved Caspase-3 (C-Casp3) antibody. The z-stack confocal images and the three-dimensional images at P11 clearly showed the drastic change in the number of GER cells (Figure 1C,D), C-Casp3-positive cells (Figure 1A, B) and the shape of GER (Figure 1E, F). In R75W + mice, the number of GER cells and the C-Casp3 positive cells were higher than in the littermate control (Figure 1A-D) and the shape of the GER displayed an immature form which was flat and thick compare with the non-Tg littermate control, which was almost same form as the adult organ of Corti with a small ridge at the neural side of the hair cells (Figure 1E-H).

Histological analysis of the GER

Apical turns of the cochleae were observed with cross sections. Histological examinations of H-E-stained cochlear sections revealed no gross differences in GER morphology between R75W + mice and non-transgenic (non-Tg) controls at P8 (Figure 1A,B). In both R75W + and non-Tg mice, a number of cells within the GER exhibited apoptotic characteristics (e.g., chromatin condensation) at P8 (Figure 1A,B, arrows). At P12, GER cells were clearly present in non-Tg mice, but both the number of cells in the GER and the area of the GER were visibly reduced compared to P8 (Figure 1C), and no apoptotic cells were detected. In contrast, there was less reduction in the GER size and apoptotic cells were visible in R75W + mice at P12 (Figure 1D, arrow).

TEM studies also revealed differences between non-Tg and R75W + mice at P12 (Figure 1E,F). Nuclei with highly condensed chromatin were detected in retained GER cells only in R75W + mice (Figure 1F, arrow). TEM images also indicated that the GER of R75W + mice at P12 was larger, both in cell number and in total area, than that of non-Tg mice (Figure 1E,F region within dotted line).

Area of the GER

Total area of the GER was measured in non-Tg and R75W + mice at P8, P10, and P12 as illustrated in Figure 2 (see dotted area). When comparisons between time points were performed for either non-Tg mice or R75W + mice, no significant differences in GER size were detected (Figure 3). In comparisons between non-Tg and R75W + mice at P8 and P10, GER areas tended to be larger in R75W + mice, although these differences were not significant (Figure 3). At P12, however, the area of the GER was significantly larger in R75W + mice than in non-Tg mice ($p = 0.043$).

Number of cells in the GER

The total number of cells in the GER was counted for both non-Tg and R75W + mice at P8, P10, and P12 as illustrated in Figure 2 (see red line). When comparisons were made between non-Tg and R75W + mice at the three time points, no significant differences in cell number were detected at P8 or P10 (Figure 4). At P12, however, the GER of non-Tg mice had significantly fewer cells than the GER of R75W + mice ($p = 0.050$, Figure 4). The GER of non-Tg mice had 5–9 cells per section, whereas the GER of R75W + mice retained 12–24 cells per section (Figure 4).

Apoptotic cells in the GER

At P8, a small number of GER cells exhibited apoptotic characteristics (e.g., chromatin condensation) in both non-Tg and R75W + mice. In non-Tg mice the number of apoptotic cells declined after P8, with almost no apoptosis detected at P12 (Figure 5). In contrast, there were no significant differences in apoptotic nuclei in R75W + mice, and apoptotic nuclei were still detected in at the P12 time point. When the number of apoptotic cells in the GER was compared between non-Tg and R75W + mice, a significant difference was detected at P12 ($p = 0.014$; Figure 5).

Discussion

In this study, we found elevated levels of programmed cell death in the GER of R75W + mice at P12 and the retention of GER at the same time.

The loss or impairment of gap junction-mediated intercellular communication has been associated with tumor progression in a number of contexts. Reduced expression of gap junction genes has been demonstrated in several human cancers, including gastric cancer (*CX32*) [14], prostatic adenocarcinoma (*CX43*) [15], brain glioma (*CX43*) [16], breast cancer (*CX43*) [17], and lung cancer (*CX32* and *CX43*) [18]. When these gene functions are restored, cell growth slows and more normal

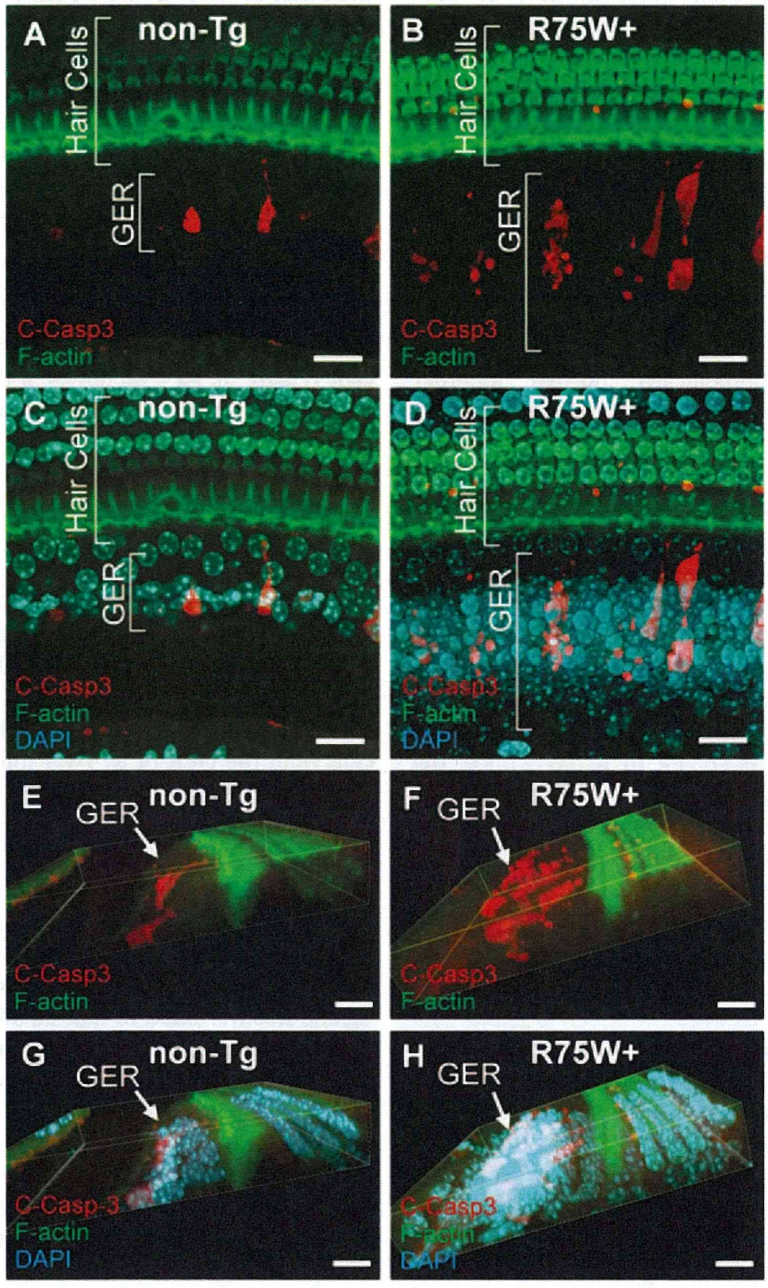

Figure 1 Difference in programmed cell death with the activation of Caspase-3 in the GER of R75W + mouse at P11. At P11, whole mount cochlear tissue of R75W + mice and the littermate controls was immunolabeled by anti-Cleaved-Caspase-3 (red, C-Casp3) with Phalloidin for F-actin (green) and DAPI for the nucleus (light green). Fifty slices of *z*-stack confocal images for the organ of Corti were collected at 0.5 μm intervals (total 25.5 μm depth from the surface of the organ of Corti). **(A-D)** The single image stacks for R75W + mouse **(B, D)** and the littermate controls **(A, C)** were constructed with LSM Image Browser (Zeiss). C-Casp3 and F-actin labelings are shown with **(C, D)** or without **(A, B)** nuclear labeling. **(E-H)** Three-dimensional images were constructed with the above confocal images of C-Casp3 and F-actin labeling with **(G, H)** or without **(E, F)** nuclear labeling. Bars indicate 20 μm.

phenotypes arise [19,20]. Thus, *connexins* are generally considered tumor suppressor genes [21]. Transfection of *CX26* into a tumor cell lines typically results in growth suppression [22-24].

Connexins have also been associated with programmed cell deatz [25,26]. In colorectal cancer cells, positive associations have been identified between *CX26* and the pro-apoptotic gene *BCL2-associated X protein* (*BAX*) and between *CX26* and the anti-apoptotic gene *BCL2-like 1* (*BCL2L1*) [27]. Wild-type gap junctions help regulate cellular growth, differentiation, tissue development, and apoptosis [28]. Finally, aberrant DNA methylation of the *CX26*

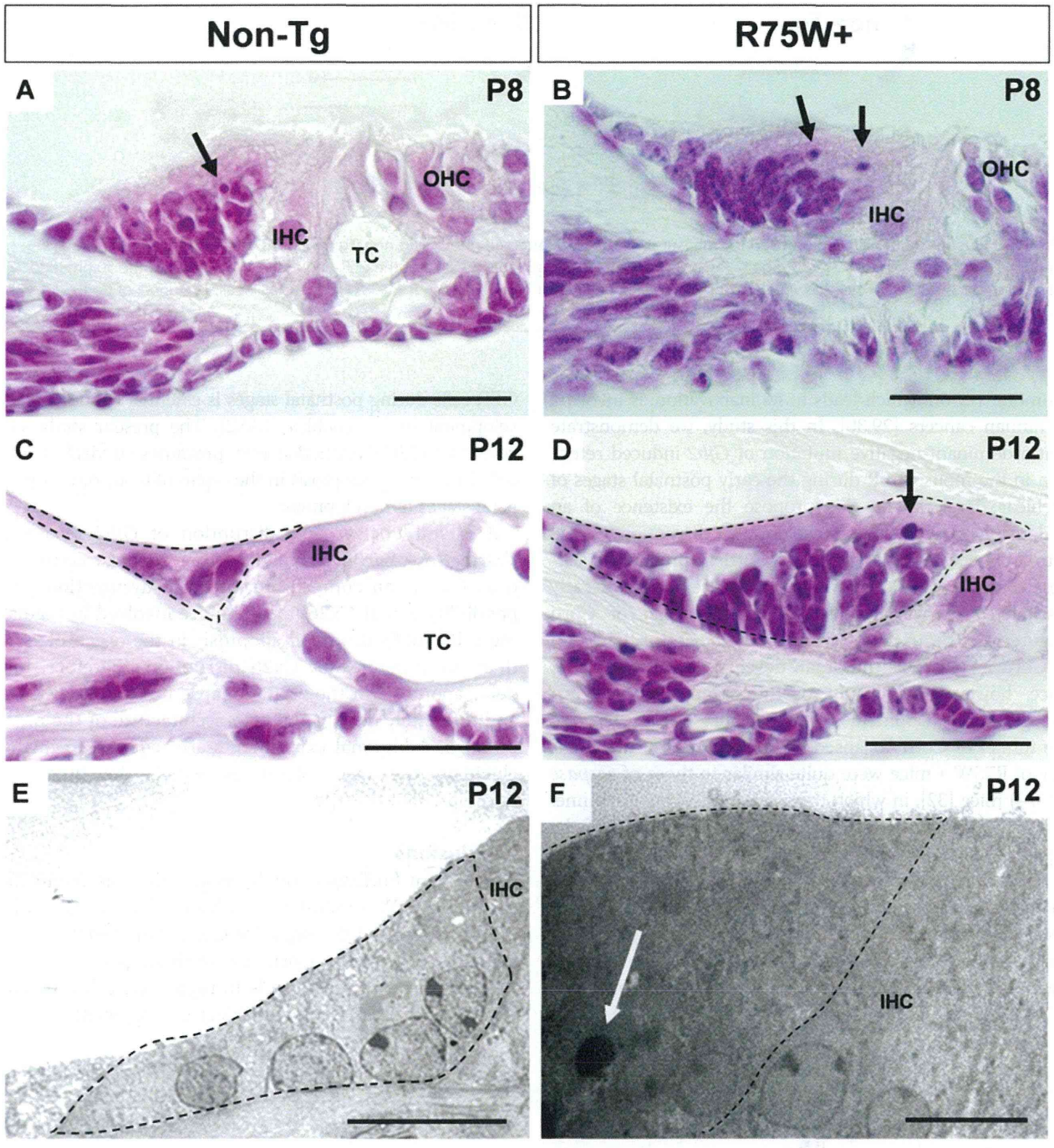

Figure 2 Morphological analysis of the GER in R75W + transgenic mice. (A-D) Hematoxylin and eosin staining of cochlear sections from R75W + and non-transgenic (non-Tg) mice. Apical turns in the cochlear were observed using microscopy. At P8, a fraction of the GER cells showed apoptotic characteristics (e.g., chromatin condensation) in both non-Tg and R75W + mice (**A**, **B**, arrows). IHC and OHC were detected in both non-Tg and R75W + mice **(A, B)**. TC was detected in non-Tg **(A)**, but not in R75W + **(B)**. At P12, the GER of non-Tg mice had 5–9 cells per section and no apoptosis **(C)**. In contrast, the GER (dotted line in D) of R75W + mice had 12–24 cells per section and had condensed nuclei indicative of apoptosis (**D**, arrow). TC is widely opened in non-Tg **(C)**, but is not detected in R75W + **(D). (E, F)** TEM images at P12 revealed no degenerative changes in non-Tg mice **(E)**, but nuclei with highly condensed chromatin were present in the enlarged GER of R75W + mice (**F**, arrow). The dotted line for C-E indicates the area of the GER. IHC, inner hair cell; OHC, outer hair cell; TC, tunnel of Corti. Scale bars = 25 μm **(A–D)** or 10 μm **(E, F)**.

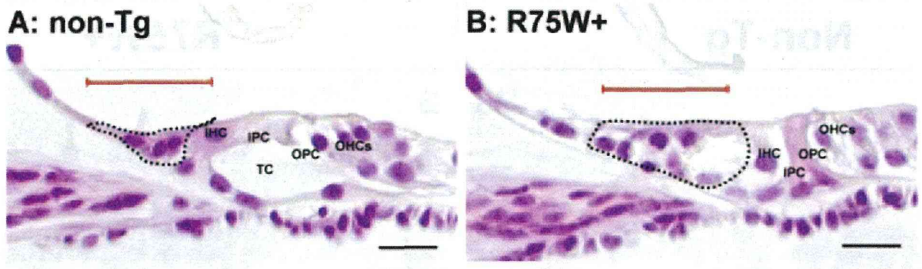

Figure 3 Illustration of GER region used for measurement of area and cell number in non-Tg (A) and R75W + (B) mice at P12. Apical turn in the cochlear were observed using microscopy. The dotted line indicates the area of the GER, and the red line indicates the 50-μm-long region in which cells were counted. IPC, inner pillar cell; OPC, outer pillar cell; IHC, inner hair cell; OHC, outer hair cell; TC, tunnel of Corti. Scale bars = 50 μm.

promoter region, which leads to its inactivation, is involved in human cancers [29,30]. In this study, we demonstrate that a dominant-negative mutation of *Gjb2* induced retention in the mouse GER during the early postnatal stages of cochlear development. We propose the existence of an underlying mechanism to explain the disruption of the cyto-architecture in the organ of Corti in prelingual deafness caused by the *Gjb2* mutation (Figure 6). This clearly disrupted the cyto-architecture of the organ of Corti (Figure 1D, 2B). In wild-type mice, the height of the organ of Corti increases as the organ develops [31]. In R75W + mice, however, the height of the organ remained unchanged as development progressed, presumably because the tunnel of Corti collapsed [6]. In this regard, the cochleae of R75W + mice were quite similar to those of *caspase 3* (−/−) mice [32], in which the space that forms the tunnel of Corti is known to collapse, reducing the height of the organ of Corti. We have previously shown GER retention in mice that lack *caspase 3* [32]. The enlarged GER that characterizes *caspase 3* (−/−) mice may result from diminished apoptosis and/or elevated levels of cell proliferation during embryogenesis. Most apoptosis within the developing cochlear system of the mouse occurs during embryogenesis [11]. We have demonstrated, however, that apoptosis of GER cells during postnatal stages is essential for normal development of the cochlea [13,32]. The present study suggests that *Gjb2* dysfunction may promotes survival of GER cells by delaying apoptosis in the organ of Corti during postnatal stages of development.

It is still unclear why disruption of *Gjb2* results in hearing loss, particularly when other cochlear connexins (e.g., Cx30) can compensate for Cx26 dysfunction. One possibility is that Cx26 may be more involved in regulating cell proliferation and apoptosis in the organ of Corti than other connexins. Cx26 disruption, therefore, may delay apoptosis in the GER, collapse the tunnel of Corti, and ultimately disrupt the cyto-architecture of the organ of Corti. Additional experiments are required to further elucidate the mechanisms by which the inner ear develops.

Conclusions

The present findings strongly suggest that the dominant-negative R75W + mutation of *Cx26* delays programmed cell death around the organ of Corti. This results in collapse of the organ of Corti. These findings indicate that CX26 may play a critical role in regulating cell proliferation and apoptosis during cochlear development.

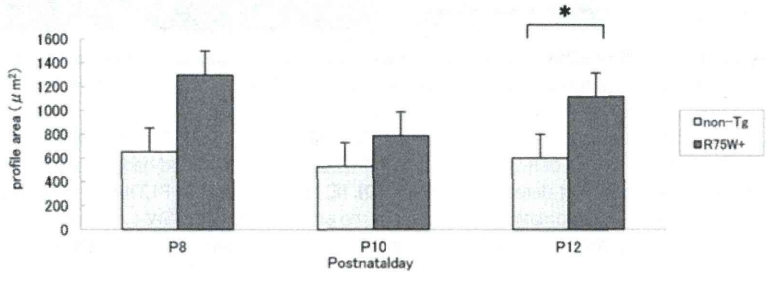

Figure 4 Area of the GER as a function of age. We examined GER areas in non-Tg and R75W + mice at P8 (n = 5), P10 (n = 5), and P12 (n = 5). For both non-Tg and R75W + mice, there were no significant differences among P8, P10, and P12. Between non-Tg and R75W + mice, the GER was significantly larger in R75W + mice at P12 (*$p \leq 0.05$). These data are expressed as mean ± SEM.